Variable Conductance Heat Pipes: A First-Order Model

R. P. Bobco*
Hughes Aircraft Company, Los Angeles, California

The variable-conductance heat pipe (VCHP) is modeled as a one-dimensional fin with a discrete heated zone between unknown axial locations l_1 and $-l_0$. The length l_1 is constrained by the distribution of noncondensable gas throughout the length of the pipe and in a temperature-controlled, wicked reservoir; the length $-l_0$ must be determined empirically. Internal heat and mass transfer processes are subsumed by postulating that condensation imposes a specified local heat flux in the heated zone only. An analytically tractable heat flux distribution is assumed by introducing a parameter s that must be determined either empirically or intuitively. The heat pipe operates in a steady state and loses energy either by convection or linearized radiation, with different values of heat loss coefficient in the active and inactive condenser zones. A closed-form solution for axial temperature is found in terms of heat load, reservoir temperature, environmental conditions, wick/wall thermal conductance, the two parameters $(-l_0, s)$, and the condensation front location l_1. An algebraic expression for the condensation front is obtained from the noncondensable gas inventory; the mass distribution integral is decomposed into zonal integrals and each integral is evaluated by a mean value approximation based on mean zonal temperature. The temperature and condensation front equations must be solved simultaneously to predict VCHP performance. Data of Edwards and Marcus are used to evaluate the empirical constants $(-l_0, s)$. An example is included to illustrate how the formulation may be used to predict diffusion freezeout and specify the gas reservoir volume.

Nomenclature

A_c = condenser cross-sectional area for vapor/gas transport, m^2
A_w = conduction cross-sectional area of wick plus wall, m^2
b = transport parameter, $(Bil_3/\delta_w)^{\frac{1}{2}}$, nondimensional
Bi = hl_3/k_w, Biot modulus, nondimensional
$f(z)$ = nondimensional heat flux distribution
h = local heat loss coefficient, W/m^2 · K
H = hSl_3, condenser heat loss coefficient, W/K
k_w = mean thermal conductivity of wick and wall structure, W/m · K
l = axial length, m
L_j = nondimensional length of jth zone, l_j/l_3
m_g = mass of noncondensable gas, kg
p_g = gas partial pressure, N/m^2
p_v = vapor partial pressure, N/m^2
q = local heat flux, $q_0 f(z)$, W/m^2
q_0 = reference heat flux, Eq. (6), W/m^2
Q = heat load applied to evaporator, W
R_g = gas constant, N · m/kg · K
s = heat flux distribution parameter, nondimensional
S = pipe periphery, m
T = local axial temperature, K
T_∞ = environmental (ambient) temperature, K
V_c = condenser plus secondary adiabatic section volume occupied by vapor/gas, m^3
V_r = reservoir volume, m^3
z = axial location, m
δ_w = equivalent wall thickness, A_w/S, m
ζ = nondimensional axial location, z/l_3
ϕ = nondimensional temperature $(T - T_\infty)/(q_0 l_3/k_w)$
ψ = gas density parameter, $p_g(Te, T)/T$, N/m^2 · K

Subscripts and Superscripts

a = active condenser section
e = evaporator
i = inactive condenser section
$\bar{(\,)}_j$ = mean value in jth section
$\tilde{(\,)}$ = hot case
$\hat{(\,)}$ = cold case

Received March 21, 1985; presented as Paper 85-0935 at the AIAA 20th Thermophysics Conference, Williamsburg, VA, June 19-21, 1985; revision received Dec. 15, 1985.

*Senior Scientist, Space and Communications Group. Associate Fellow AIAA.

Background

A SERIOUS impediment to the widespread use of the variable-conductance heat pipe (VCHP) for thermal control applications is that no simple analytical model exists for predicting evaporator temperature as a function of heat load under varying environmental conditions. For spacecraft applications, a thermal designer must deal with several problems when specifying a VCHP. The primary problem is maintaining power-dissipating equipment within a prescribed temperature range under a variety of power dissipation levels and during diurnal-to-seasonal changes in environmental conditions. Secondary problems include the need for a low-mass reservoir specified for noncondensable gas, requirements to use minimal power for keeping the gas reservoir within a specified temperature range, and the fact that diffusion freezeout must be avoided when operating at low heat loads.

Both empirical and analytical methods are available to the thermal designer. Empirical methods based on tests in space simulation chambers in the Earth gravity field are expensive and not always satisfactory. Analytical methods based on diffuse front[1-3] and flat front models require computer codes, thermophysical data banks, and insights that are not always available.

The elegant diffuse front model of Edwards and Marcus[1,2] and the modifications of Shimoji et al.[3] are not readily applicable to nodal models of spacecraft equipment shelves. Their iterative, simultaneous solution of heat and mass transport equations and the noncondensable gas inventory of nodal models require a geometric model with high axial resolution. Their model also requires certain thermophysical data that are not easily found. Evaporation and condensation film coefficients and radial and axial conductances in capillary wick structures are not public data for most common heat pipe

fluids and materials. A flat front code, adapted from GASPIPE algorithms,[4] was tested recently at Hughes Aircraft Company and found to be both slow and marginally convergent when used as a subroutine for an analytical model with several hundred nodes (e.g., equipment, shelf radiator, multiple VCHPs). The flat front model shares with the diffuse front model the uncertainty of selecting internal film coefficients and conductances and the need for an iterative solution to satisfy thermal and gas inventories simultaneously. Moreover, the heat pipe model was "stiff" insofar as evaporation and condensation coefficients were very large and wall-to-fluid temperature differences very small.

A simple, first-order analytical model is described here that should be useful for formulating preliminary design and for use as a teaching device. Also, it is believed that the concepts underlying the closed form may be adapted to computer codes. This model is based on two independent simplifying assumptions: 1) the internal convection process associated with condensation is replaced by a specified local heat flux; and 2) the distribution of noncondensable gas throughout the length of the heat pipe and in the gas reservoir is calculated in terms of mean temperatures in the several regions. An isolated VCHP is modeled in terms of the linear, one-dimensional, fin equation and a closed-form solution for the temperature distribution is found in terms of a parameter L_1 that defines the location at which condensation is complete. The parameter L_1 corresponds to the location of the flat front and an algebraic expression for L_1 is formulated from the mass balance on the noncondensable gas. An iterative solution is required to solve for evaporator temperature T_e and L_1 simultaneously. The formulation is validated by using experimental data reported by Edwards and Marcus.[1,2]

Assumptions and Analysis

The geometry of the VCHP examined here is shown in Fig. 1. It is convenient to subdivide the heat pipe into seven functional zones as shown in the figure. Only the region $-l_0 < z < l_3$ and the gas reservoir are modeled here.

Assumptions are as follow: 1) the wick extends the length of the heat pipe and into the reservoir; 2) the reservoir and the end of the pipe at $z = l_3$ are at a controlled temperature T_r; 3) axial conduction is negligible at $z = -l_0$; i.e., $dT/dz = 0$; 4) negligible gas is in the region $z < -l_0$; 5) condensation (i.e., heat release) of working fluid occurs in region $-l_0 < z \le l_1$ only; 6) the vapor, gas, and structure (i.e., wick and wall) temperatures are identical at any axial location; 7) noncondensable gas behaves like a perfect gas, $p_g V = m_g R_g T$; 8) total pressure is constant everywhere in $-l_0 < z \le l_3$ and in the reservoir; 9) axial heat transfer occurs by conduction in the wick/wall structure; radial heat transfer occurs at the exposed pipe surface ($0 < z \le l_2$), either by convection or by linearized radiation; 10) no heat is lost radially in evaporator and adiabatic sections; and 11) the heat load and environmental conditions are steady.

Within the framework of these assumptions, the analysis proceeds by satisfying the principles of mass and energy conservation simultaneously. The mass of noncondensable gas must satisfy the relation

$$m_g = \left(\frac{p_g V}{R_g T}\right)_{\text{res}} + \int_{V(-l_0)}^{V(l_3)} \frac{p_g \, dV}{R_g T} \tag{1}$$

while energy conservation is satisfied by the one-dimensional fin equation

$$k_w A_w \frac{d^2 T}{dz^2} - Sh(z)(T - T_\infty) = -Sq(z) \tag{2}$$

and the obvious heat balance

$$Q_{\text{evap}} = S\int_{-l_0}^{l_1} q(z)\, dz \tag{3}$$

It should be observed that neither the heat flux distribution $q(z)$ nor the location l_0 are known a priori.

The gas pressure in Eq. (1) must be found from the law of partial pressures

$$p_g(T_e, T) = p_v(T_e) - p_v(T) \tag{4}$$

where the total pressure corresponds to the pressure of saturated vapor in the evaporator at temperature T_e and the vapor pressures may be found from tables or correlating equations.[5]

The analysis starts by introducing nondimensional parameters and assuming a discontinuous condensation flux of the form,

$$\begin{aligned} f(\zeta) &= 1, && -L_0 < \zeta \le 0 \\ &= 1 + s\zeta^n, && 0 < \zeta \le L_1 \\ &= 0, && L_1 < \zeta \le 1 \end{aligned} \tag{5}$$

where s must be evaluated empirically. These equations allow the reference flux to be evaluated from Eq. (3) as

$$q_0 = Q \Big/ \left[Sl_3 \left(L_1 + |L_0| + \frac{sL_1^{n+1}}{n+1} \right) \right] \tag{6}$$

Also, it is assumed that the external film coefficients differ in the active and inactive condenser sections as

$$\begin{aligned} h(\zeta) &= h_a, && 0 < \zeta \le L_1 \\ &= h_i, && L_1 < \zeta \le L_2 \end{aligned} \tag{7}$$

The piecewise continuous nature of $q(z)$ and $h(z)$ suggests a need to obtain zonal solutions of Eq. (2). The fin equation is decomposed into nondimensional form

$$\frac{d^2\phi_0}{d\zeta^2} = \frac{-l_3}{\delta_w}, \qquad -L_0 < \zeta \le 0 \tag{8a}$$

$$\frac{d^2\phi_1}{d\zeta^2} - b_a^2\phi_1 = -\frac{(1 + s\zeta^n) l_3}{\delta_w}, \qquad 0 < \zeta \le L_1 \tag{8b}$$

$$\frac{d^2\phi_2}{d\zeta^2} - b_i^2\phi_2 = 0, \qquad L_1 < \zeta \le L_2 \tag{8c}$$

$$\frac{d^2\phi_3}{d\zeta^2} = 0, \qquad L_2 < \zeta \le 1 \tag{8d}$$

The boundary conditions are

$$\zeta = -L_0, \quad \frac{d\phi}{d\zeta} = 0; \qquad \zeta = 1, \quad \phi = \phi_r \tag{9}$$

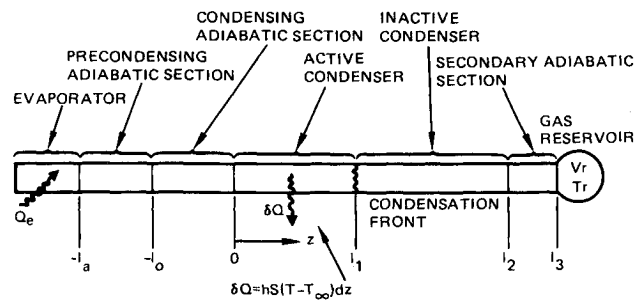

Fig. 1 Schematic of VCHP showing functional zones and coordinate system.

At the interfaces $\zeta = 0$, L_1, and L_2 the solutions must match in temperature and conserve energy,

$$\zeta = \zeta_j : \phi(\zeta_j^-) = \phi(\zeta_j^+)$$
$$\phi'(\zeta_j^-) = \phi_j'(\zeta_j^+) \tag{10}$$

This zonal formulation for a VCHP is comparable to that used by Sun and Tien[6] for a fixed-conductance heat pipe. When the exponent n is an integer, the solutions of Eq. (8) may be found in closed form; for convenience, the remaining analysis will be limited to the case $n = 2$. The boundary conditions lead to the results

$$B_0 = -|L_0|(l_3/\delta_w), \qquad B_3 = \phi_r - A_3 \tag{11a}$$

and temperature and flux matching at $\zeta = 0$ provide

$$A_0 = \phi_1(0), \qquad B_1 = -b_a|L_0|/Bi_a \tag{11b}$$

The remaining constants of integration must be evaluated from the matching conditions at $\zeta = L_1$ and L_2,

$$\begin{vmatrix} \cosh b_a L_1 & -\cosh b_i L_1 & -\sinh b_i L_1 & 0 \\ b_a \sinh b_a L_1 & -b_i \sinh b_i L_1 & -b_i \cosh b_i L_1 & 0 \\ 0 & \cosh b_i L_2 & \sinh b_i L_2 & -(1-L_2) \\ 0 & b_i \sinh b_i L_2 & b_i \cosh b_i L_2 & 0 \end{vmatrix}$$
$$\times \begin{vmatrix} A_1 \\ A_2 \\ B_2 \\ A_3 \end{vmatrix} = \begin{vmatrix} \frac{-1}{Bi_a}\left[1 + s\left(L_1^2 + \frac{2}{b_a^2}\right) - b_a|L_0|\sinh b_a L_1\right] \\ \frac{-1}{Bi_a}\left[2sL_1 - b_a^2|L_0|\cosh b_a L_1\right] \\ \phi_r L_2 \\ \phi_r \end{vmatrix} \tag{12}$$

The solutions for A_1, A_2, B_2, and A_3 may be found in closed form, but they are unwieldy. It is more practical to leave the solution in the form,

$$\phi_0(\zeta) = \phi_1(0) - (l_3/\delta_w)\left(L_0\zeta + \tfrac{1}{2}\zeta^2\right) \tag{13a}$$

$$\phi_1(\zeta) = \frac{1}{Bi_a}\left[1 + s\left(\zeta^2 + \frac{2}{b_a^2}\right) - b_a L_0 \sinh b_a \zeta\right] + A_1 \cosh b_a \zeta \tag{13b}$$

$$\phi_2(\zeta) = A_2 \cosh b_i \zeta + B_2 \sinh b_i \zeta \tag{13c}$$

$$\phi_3(\zeta) = A_3(1-\zeta) + \phi_r \zeta \tag{13d}$$

and to invert the matrix of Eq. (12) numerically.

Equations (12) and (13) represent the temperature field for a VCHP operating with a nominal heat load that drives the condensation front into the region $0 < \zeta \le L_2$; however, at very low heat loads, all of the condensation may occur within the adiabatic section $-L_0 < \zeta \le 0$. For this case, the fin equation takes the zonal form

$$\phi_0'' = -l_3/\delta_w, \qquad -L_0 < \zeta \le -L_1 \tag{14a}$$
$$\phi_1'' = 0, \qquad -L_1 < \zeta \le 0 \tag{14b}$$
$$\phi_2'' - b_i^2 \phi_2 = 0, \qquad 0 < \zeta \le L_2 \tag{14c}$$
$$\phi_3'' = 0, \qquad L_2 < \zeta \le 1 \tag{14d}$$

where it is assumed that the entire condenser length is inactive. Using $f(\zeta) = 1$ in $-L_0 < \zeta \le -L_1$ and $f(\zeta) = 0$ for $\zeta > -L_1$, Eq. (3) gives

$$q_0 = Q/[Sl_3(|L_0| - |L_1|)] \tag{15}$$

The temperature field may be expressed in reasonably concise closed form, but the equations are not shown here because they are still unwieldy. Additional analytical details are available in Ref. 7 for both very low heat load and nominal range performance.

The temperature $T(\zeta)$ is recovered from either Eq. (13) or the solution of Eq. (14) as

$$T_j(\zeta) = T_\infty + \left(\frac{q_0 l_3}{k_w}\right)\phi_j(\zeta), \qquad j = 0,1,2,3 \tag{16}$$

From the third assumption, it may be inferred that the evaporator temperature T_e is identical to the temperature at the location $\zeta = -L_0$; that is,

$$T_e = T(-L_0) = T_\infty + \left(\frac{q_0 l_3}{k_w}\right)\phi_0(-L_0) \tag{17}$$

From Eqs. (13) and (6) for nominal heat loads, find values described by Eq. (18). Equation (18) provides a direct relationship between evaporator temperature T_e and evaporator heat load Q when L_1, L_0, and s are known.

$$T_e = T_\infty + Q\left[\frac{(1 + 2s/b_a^2)/hSl_3 + A_1/k_w S + \frac{1}{2}L_0^2/(k_w A_w/l_3)}{|L_0| + L_1 + sL_1^3/3}\right] \tag{18}$$

A comparable expression may be obtained for cases of very low heat load.[7]

The noncondensable gas inventory developed by Eq. (1) may be used to develop a first-order expression for L_1. Let $dV = A_c l_3 d = V_c d\zeta$ and, for a nominal heat load, decompose the integral in Eq. (1) as shown in Eq. (19),

$$\int_{V(-L_0)}^{V(L_3)}\left(\frac{p_g\, dV}{R_g T}\right) = \frac{V_c}{R_g}\left[\int_{-L_0}^{0} + \int_0^{L_1} + \int_{L_1}^{L_2} + \int_{L_2}^{1}\left(\frac{p_v(T_e) - p_v(T)}{T}\right)d\zeta\right] \tag{19}$$

The integrals of $p_v[T(\zeta)]/T(\zeta)$ cannot be evaluated in closed form. In principle, each integral in Eq. (19) may be evaluated in the form

$$\int_{\zeta'}^{\zeta''}\left[\frac{p_v(T_e) - p_v(T)}{T}\right]d\zeta = \left[\frac{p_v(T_e) - p_v(T)}{T}\right]_{\text{mean}} \times (\zeta'' - \zeta') \tag{20}$$

As a first-order approximation, it is assumed that the mean value of the integrand may be evaluated at the mean temperature in the interval as shown in Eqs. (21a) and (22b) and $T(\zeta)$ is given by Eq. (13).

$$\left[\frac{p_v(T_e)-p_v(T)}{T}\right]_{\text{mean}} \approx \frac{p_v(T_e)-p_v(\bar{T})}{\bar{T}} = \frac{p_g(T_e,\bar{T})}{\bar{T}} \tag{21a}$$

where

$$\bar{T} = \frac{1}{\zeta''-\zeta'}\int_{\zeta'}^{\zeta''} T(\zeta)\,d\zeta \tag{21b}$$

Using equations (19-21) in Eq. (1) leads to an explicit expression for the parameter L_1 for nominal heat loads shown in Eqs. (22).

$$L_1 = \frac{\left[\psi_r\frac{V_r}{V_c} + \bar{\psi}_0|L_0| + \bar{\psi}_2 L_2 + \bar{\psi}_3(1-L_2)\right] - \frac{m_g R_g}{V_c}}{(\bar{\psi}_2 - \bar{\psi}_1)} \tag{22a}$$

in which

$$\psi_j = \frac{p_g(T_e,T_j)}{T_j}, \qquad \bar{\psi}_j = \frac{p_g(T_e,\bar{T}_j)}{\bar{T}_j} \tag{22b}$$

The corresponding expression for very low heat loads is

$$|L_1| = \frac{\left[\psi_r\left(\frac{V_r}{V_c}\right) + \bar{\psi}_0|L_0| + \bar{\psi}_2 L_2 + \bar{\psi}_3(1-L_2)\right] - \frac{m_g R_g}{V_c}}{(\bar{\psi}_0 - \bar{\psi}_1)} \tag{23}$$

Equations (18) and (22) must be solved simultaneously when L_0 and s are known. Current information on the magnitudes of s and L_0 are meager. Intuition suggests two characteristics, based on observed temperatures, of the magnitude of s: 1) the temperature must be virtually isothermal over a large portion of the region $0 < \zeta < L_1$; and 2) a temperature maximum in the same region is improbable. With regard to L_0, intuition suggests that for nominal heat loads, L_0 will be small because the temperature in the region $-L_0 < \zeta < 0$ should be virtually isothermal. At very low heat loads, there is no intuitive guideline to the magnitude of L_0. Additionally, it is reasonable to expect that both s and L_0 may be influenced by thermal conductivity k_w and environmental conditions h_a, h_i, and T_∞.

Validation Analysis

This formulation provides a closed-form, implicit relation among heat load Q, evaporator temperature T_e, and the condensation front parameter L_1. However, the formulation is based on two gross simplifications (the flux-driven fin equation and the mean value gas balance) and the introduction of two impalpable parameters, L_0 and s. In recognition of the tentativeness of the formulation, the experimental data of

Table 1 Heat pipe design details[1,2]

Parameter	Specification
Working fluid	Water
Inert gas	Air ($2.67 \times 10^{-6} \pm 5\%$ lb · mole)
Pipe	
Material	Stainless steel
Outside diameter	14.4 mm (0.565 in.)
Wall thickness	0.914 mm (0.036 in.)
Overall length	1.39 m (54.75 in.)
Condenser length	0.768 m (30.25 in.)
Evaporator heat input length	0.318 m (12.5 in.)
Adiabatic section length	0.305 m (12.0 in.)
Wick structure	
Material	200 mesh stainless steel screen
Description	Concentric annulus artery (0.015 in. gap width) with 2 wraps of screen held in place by a spring.

Heat loss coefficients

T_e		T_∞		h	
K	(R)	K	(R)	W/m² · K	(Btu/h · ft · R)
411.1	(740)	298.2	(536.7)	20.8	(3.66)
379.2	(682.5)	298.2	(536.7)	18.3	(3.23)
370.6	(667.1)	297.7	(535.8)	18.2	(3.21)
354.2	(637.6)	297.2	(534.9)	16.6	(2.92)

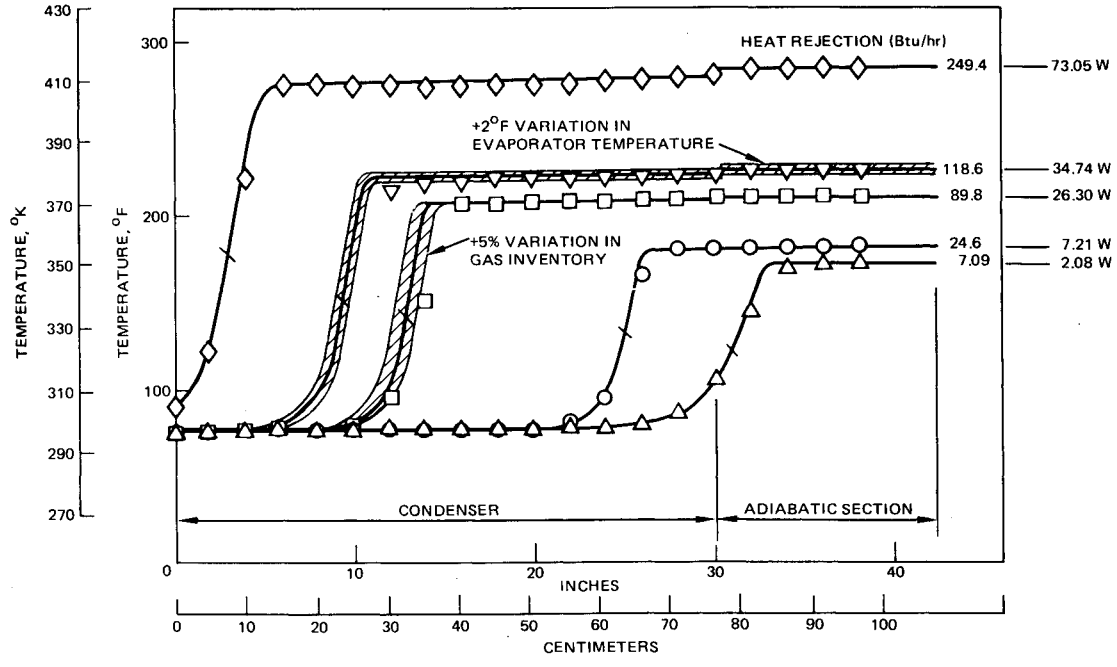

Fig. 2 Comparison of measured and predicted temperature profiles for a gas-loaded heat pipe (Refs. 1 and 2).

Edwards and Marcus[1,2] were used to validate the formulation and gain insight to the magnitudes of L_0 and s.

Edwards and Marcus report the performance of a stainless steel VCHP using water as the working fluid and air as the noncondensable gas. They present heat pipe design details, measured values of combined free convection/radiation film coefficients, graphical axial temperature distributions for five heat loads, and a graph showing heat load as a function of evaporator temperature. This information is repeated here as Table 1. Their report shows that the experimental VCHP had neither a secondary adiabatic section nor a temperature controlled reservoir (i.e., $V_r = 0$). Edwards and Marcus report that the evaporator and adiabatic sections were insulated with "2 inches of polyurethane foam," but do not provide data on the effective axial thermal conductivity of the wick structure, the effective void cross-sectional area A_c, or the value of pipe thermal conductivity used in their analytical predictions.

The analysis, text, tables, and figures in Ref. 1 are virtually identical to Sec. 6.3 of Ref. 2. A notable difference between the two references appears in the legends of the figures captioned "Comparison of predicted and observed heat transfer rates as a function of heat pipe evaporator temperature." In Ref. 1, the legend shows "Test data (corrected for evaporator insulation losses)"; in Ref. 2 the legend states "Test data (corrected for insulation losses)." Although the different parenthetical statements are similar, it is uncertain whether the test data were corrected for adiabatic section losses. It will be seen, below, how this uncertainty is propagated in the validation analysis.

The axial temperature distributions[2] are reproduced here in Fig. 2. These data were used to estimate the location of the front by assuming $T(l_1) = 0.5(T_e + T_r)$. Table 2 summarizes the best estimate at interpreting the published data. Also included in Table 2 are the film coefficients, heat loads (both as published and corrected for adiabatic section heat leaks), transport parameters, and temperatures for each run. It was assumed that the film coefficients of Table 1 applied for runs 1-4. The film coefficient for run 5 (very low power) was estimated by graphical extrapolation from the original four values. The heat loss from the adiabatic section δQ was estimated by using $k_{ins} = 0.012$ W/m · K for polyurethane foam and the appropriate film coefficient to evaluate an overall conductance,

$$UA = 2\pi l_a \left[\ell n(r_2/r_1)/k_{ins} + 1/hr_2 \right]^{-1}; \qquad l_a = 0.305 \text{ m}$$

The environment temperature was taken as $T_\infty = 297$ K. The thermal conductivity of the wick was neglected and $k_w = 5.43$ W/m · K was used for the stainless steel pipe wall. In addition, it was assumed $V_r = 0$ and $L_2 = L_3 = 1$.

The validation analysis proceeded in three distinct steps:

1) Temperature profile verification. Trial-and-error calculations were made to find the magnitudes of (L_0, s) that provided the best match for T_e, L_1, and the temperature profiles of Fig. 2. It was found that the values $(L_0, s) = (0, 0)$ provided the best match for nominal heat loads (both as published in Refs. 1 and 2 and corrected for heat leaks in the adiabatic section). The single data point at very low heat load (run 5) was more difficult to match; an acceptable match was found by varying the set $(Q_{e,\text{corr}}, L_0)$ with the result $Q_{e,\text{corr}} = 0.276$ W, $L_0 = 0.1983$. In consideration of the tentative status of the formulation at very low heat loads, it was concluded that the present first-order model should be confined to nominal heat loads. It is apparent that more test data are needed to understand VCHP performance at very low heat loads.

2) Estimate of condenser void volume V_c. The information in Table 1 is not sufficient to calculate the condenser void volume V_c. Equation (22a) was rearranged to solve for V_c using data for run 4 with $(s, L_0, L_1, L_2, Q) = (0, 0, 0.1752, 1, 5.36$ W). It was found that $V_c = 76.76$ cm^3.

3) Heat load/evaporator temperature. The last step in the validation analysis verified that the empirical evaluation of L_0, s, and V_c were consistent. The temperature equations and the gas inventory equation were solved simultaneously to establish evaporator temperature as a function of heat load. Simplified equations for T_e, T_1, and T_2 were programmed for a hand calculator with a vapor pressure correlation[5] in the form

$$p_v(T) = e^{f(T)}, \qquad f(T) = \sum_{n=0}^{5} C_n T^n \tag{24}$$

An interactive, iterative procedure was used to calculate T_e as a function of Q with specified boundary and environmental conditions. The calculations were initiated by assuming a value of L_1 (proportional to Q), finding the temperatures, vapor pressures, ψ parameters, and finally calculating L_1 from Eq. (22a) or (23). After comparing the input L_1 and the

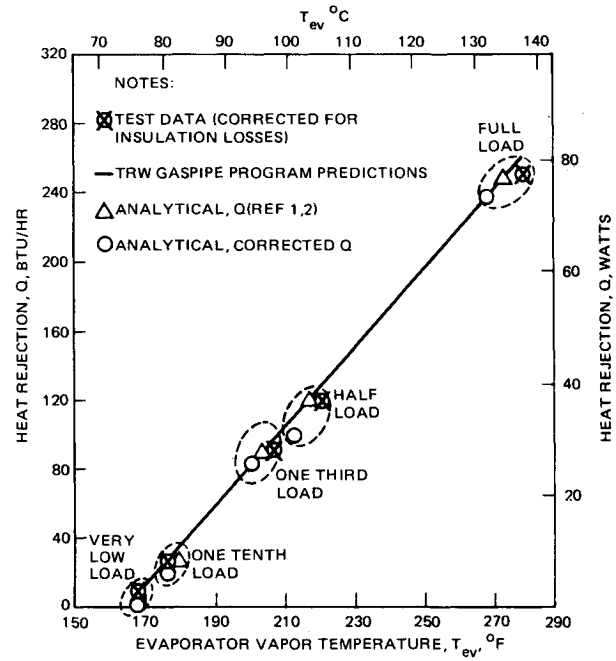

Fig. 3 Stainless/water/air VCHP (VCHP performance comparison from data in Refs. 1 and 2 and present analysis).

Table 2 Empirical data

Run	Heat Load: Published Q_e, W	Heat Load: Corrected Q_e, W	Front temperature $T[l_1]$, K	Front location l_1, m	Film coefficient h, W/m^2 · K	Transport parameter b	Evaporator temperature T_e, K	End temperature T_r, K
1	73.05	69.33	358.7	0.691	20.8	29.68	411.5	305.9
2	34.74	32.07	337.9	0.541	18.3	27.88	378.7	297.0
3	26.30	23.93	333.7	0.445	18.2	27.79	370.4	297.0
4	7.21	5.36	328.2	0.135	16.6	26.51	353.7	297.0
5	2.08	0.548	322.9	−0.015	16.2	26.23	348.7	297.0

Table 3 VCHP dimensions and operating parameters

Dimensions	
Nondimensonal condenser length	$L_2 = 0.8333$
Axial conduction area (pipe wall)	$A_w = 19.46$ mm^2 (0.0302 in.^{2})
External circumference	$S = 39.90$ mm (1.571 in.)
Equivalent wall thickness	$\delta_w = 0.702$ mm (0.0277 in.)
Wall thermal conductivity	$k_w = 5.45$ W/m · K (9.4 Btu/h · ft °R)
Vapor flow area	$A_c = 28.71$ mm^2 (0.0445 in.^{2})
NH_3 freezing temperature	$T_s = 195.5$ K (352°R)
Minimum allowable pipe temperature	$T_2^* = 197.2$ K (355°K)

Operating parameters

Parameter		Hot case		Cold case	
T_e,	K (°R)	313.9	(565)	308.3	(555)
T_∞,	K (°R)	100.0	(180)	97.2	(175)
T_r,	K (°R)	280.6	(505)	277.8	(500)
h,	W/m^2-K (Btu/h · ft^2/°R)	3.41	(0.6)	2.84	(0.5)
B_i		0.1915		0.1596	
b		15.790		14.415	
H	W/K (Btu/h · °R)	0.1242	(0.2356)	0.1036	(0.1964)
$T_r - T_\infty$	K (°R)	180.6	(325)	180.6	(325)
$T_e - T_\infty$	K (°R)	213.9	(385)	211.1	(380)

Vapor pressure[5] of NH_3 with $p = N/m^2$, $T = K$, and $p_v(T) = e^{f(T)}$ is
$f(T) = -48.05 + 0.68546T - 0.33219T^2 \times 10^{-2} + 0.8744T^3 \times 10^{-5} - 0.12019T^4 \times 10^{-7} + 0.67905T^5 \times 10^{-11}$

computed L_1, an adjusted value of L_1 was used as an input and the process was repeated until input and output values were identical. The results of these calculations appear in Fig. 3. Calculated points are shown for both published and corrected heat loads. Agreement with experimental values is good.

Reservoir Design Based on Incipient Freezeout

It is known that the temperature in the inactive condenser section may fall below the reservoir temperature when $T_\infty < T_r$ and the heat load is less than the the maximum design value. The magnitude of the minimum temperature is of special concern if the environmental temperature T_∞ is less than triple-point temperature of the heat pipe working fluid. The location of the minimum may be found from Eq. (13c) by setting the derivative equal to zero; that is, $d\phi_2/d\zeta = 0$. The location of the minimum temperature is

$$\zeta^* = \frac{1}{2b_i} \ell n \left(\frac{A_2 - B_2}{A_2 + B_2} \right) \tag{25}$$

Using this result in Eq. (13b), the magnitude of the minimum temperature, $T_2^* = T_2(\zeta^*)$, may be related to the heat load by introducing the equation

$$\frac{T_2^* - T_\infty}{\sqrt{A_2^2 - B_2^2}} = \frac{Q}{k_w S\left(|L_0| + L_1 + sL_1^3/3\right)} \tag{26}$$

It should be observed that Eq. (26) is quadratic in Q insofar as Q is implicit in A_2 and B_2.

The evaporator temperature may be expressed in terms of the minimum temperature by combining Eqs. (13a) and (26),

$$T_e = T_\infty + \left(\frac{T_2^* - T_\infty}{\sqrt{A_2^2 - B_2^2}} \right) \times \left[A_1 + \frac{1 + 2s/b_a^2}{Bi_a} + \left(\frac{l_3 S}{A_w} \right) \frac{L_0^2}{2} \right] \tag{27}$$

Equations (26) and (27) provide a basis for using incipient freezeout as one of the two conditions required to specify a gas reservoir.

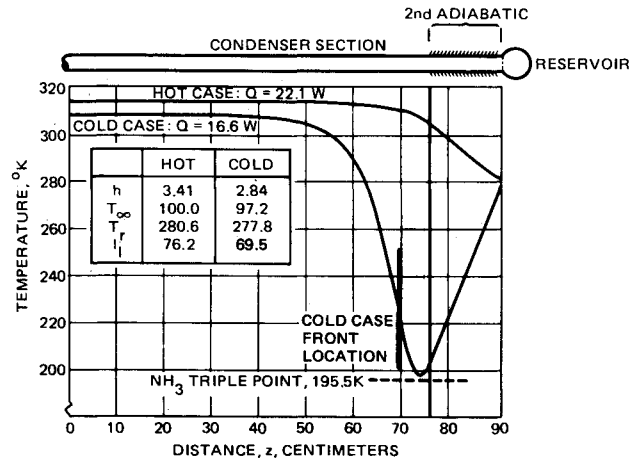

Fig. 4 Stainless/ammonia/nitrogen VCHP; temperature profiles for hypothetical VCHP at full condenser utilization (hot case) and incipient freezeout (cold case).

In a typical application for a VCHP, a designer will know the maximum heat load required for a design as well as the definitions of the extreme hot and extreme cold environments in which the VCHP must operator. The hot environment parameters are designated here with a tilda (e.g., $\psi_r = \tilde{\psi}_r$) and the cold environment parameters with a caret (e.g., $\psi_2 = \hat{\psi}_2$).

It is reasonable to expect that the condenser will be fully utilized when the VCHP operates at full load in the hot environment; that is, $\tilde{L}_1 = L_2$. The magnitude of the evaporator temperature corresponding to the maximum heat load may be found from Eq. (13a) by specifying $\tilde{Q}$, $\tilde{h}$, $\tilde{T}_\infty$, and $\tilde{L}_1 = L_2$. Also, it is reasonable to expect that diffusion freezeout is most probable when operating at a reduced heat load in the cold environment. Freezeout may be avoided by specifying a minimum allowable temperature $\hat{T}_2^*$ a few degrees above the triple point of the working fluid. Finally, the thermal designer may specify the minimum allowable evaporator temperature $\hat{T}_e$ for an application. Using $\hat{T}_2^*$, $\hat{T}_e$, $\hat{T}_\infty$, and $\hat{h}$ in Eq. (27), it is possible to find $\hat{L}_1$. The heat load necessary to avoid freezeout follows from Eq. (26). The gas inventory equation

for the hot case follows from Eq. (25a) as

$$m_g R_g = \tilde{\psi}_r V_r + V_c[\tilde{\psi}_1 L_2 + \tilde{\psi}_3(1 - L_2)], \qquad L_0 = 0 \tag{28a}$$

At incipient freezeout the gas inventory is

$$m_g R_g = \hat{\psi}_r V_r + V_c[\hat{\psi}_1 \hat{L}_1 + \hat{\psi}_2(L_2 - \hat{L}_1) + \hat{\psi}_3(1 - L_2)], \qquad L_0 = 0 \tag{28b}$$

Solving for m_g and V_r yields

$$\frac{m_g R_g}{V_c} = \frac{\{-\hat{\psi}_r[\tilde{\psi}_1 L_2 + \tilde{\psi}_3(1 - L_2)] + \tilde{\psi}_r[\hat{\psi}_1 \hat{L}_1 + \hat{\psi}_2(L_2 - \hat{L}_1) + \hat{\psi}_3(1 - L_2)]\}}{(\tilde{\psi}_r - \hat{\psi}_r)} \tag{29a}$$

$$\frac{V_r}{V_c} = \frac{\hat{\psi}_1 \hat{L}_1 - \tilde{\psi}_1 L_2 + \hat{\psi}_2(L_2 - \hat{L}_1) + (\hat{\psi}_3 - \tilde{\psi}_3)(1 - L_2)}{(\tilde{\psi}_r - \hat{\psi}_r)} \tag{29b}$$

Table 4 Simplified equations

$$T_e = T_1(0) = T_\infty + (T_r - T_\infty)(2e^{-bL}2/D) + (Q/HL_1)(1 - e^{-bL_1}) \tag{30a}$$

$$\bar{T}_1 = T_\infty + (T_r - T_\infty)(e^{-b\Delta L}/bL_1 D) + (Q/HL_1) \times \left[1 - \frac{1}{2bL_1}[1 - \bar{e}^{2b\Delta L}[1 - b(1 - L_2)]/D]\right] \tag{30b}$$

$$\bar{T}_2 = T_\infty + [(1 - e^{-b\Delta L})/b\Delta LD][T_r - T_\infty + (Q/HL_1)(1 - e^{-b\Delta L})/2] \tag{30c}$$

$$\bar{T}_3 = T_\infty + \left\{(T_r - T_\infty)\left[1 + \frac{1}{2}b(1 - L_2)\right] + \frac{(Q/HL_1)[b(1 - L_2)e^{-b\Delta L}/2]}{D}\right\}, \quad D = 1 + b(1 - L_2), \ \Delta L = L_2 - L_1 \tag{30d}$$

$$\frac{\hat{Q}}{\hat{L}_1} = \hat{H}(\hat{T}_r - \hat{T}_\infty)\left[\frac{e^{\hat{b}(L_2 - \hat{L}_1)}}{1 - \hat{b}(1 - L_2)}\right]\left\{1 - \sqrt{1 - \left[\frac{\hat{T}_2^* - \hat{T}_\infty^2}{\hat{T}_r - \hat{T}_\infty}\right]\left[1 - \hat{b}^2(1 - L_2)^2\right]}\right\} \tag{31a}$$

$$\frac{\hat{T}_e - \hat{T}_\infty}{\hat{T}_r - \hat{T}_\infty} = \frac{2e^{-\hat{b}L_2}}{1 + \hat{b}(1 - L_2)} + \left[\frac{(1 - e^{-\hat{b}\hat{L}_1})e^{+\hat{b}(L_2 - \hat{L}_1)}}{1 - \hat{b}(1 - L_1)}\right] \times \left\{1 - \sqrt{1 - \left[\frac{\hat{T}_2^* - \hat{T}_\infty^2}{\hat{T}_r - \hat{T}_\infty}\right]\left[1 - \hat{b}^2(1 - L_2)^2\right]}\right\} \tag{32b}$$

If the environmental temperature for the cold case is greater than the triple point of the working fluid, the reservoir design problem proceeds by specifying two of the three parameters ($\hat{T}e, \hat{Q}, \hat{L}_1 > 0$) and using Eq. (13a) to solve for the third. Equations (29) still apply for this more benign case.

The use of Eqs. (25-29) is illustrated below by considering a hypothetical example in which, for convenience, it is assumed that $h_a = h_i = h$.

Example

An ammonia/nitrogen gas/stainless steel heat pipe with a length of 2.135 m is required for a space application. The following length allocations are specified: evaporator, 0.1524 m; primary adiabatic section, $|l_a| = 1.067$ m; condenser, $l_2 = 0.762$ m; and secondary adiabatic section, $l_3 - l_2 = 0.1524$ m. The heat pipe manufacturer provides the following data: outer diameter × wall thickness = 12.7 × 0.746 mm; vapor flow area, $A_c = 28.71$ mm^2; thermal conductivity, $k_w = 5.43$ W/m · K; and NH_3 freezing temperature, $T_f = 195.5$ K. The heat pipe will be used in a space environment under the following extreme conditions: hot case, $(\tilde{h}, \tilde{T}_\infty) = (3.41$ W/m^2 · K, 100 K); cold case, $(\hat{h}, \hat{T}) = (2.84$ W/m^2 · K, 97.2 K). The application requires an evaporator operating in the range $T_e = 311.1 \pm 2.78$ K. Find the maximum heat load for the hot case, the minimum heat load for the cold case, the gas reservoir volume, and the nitrogen gas mass.

The environmental temperature is much less than the freezing point of ammonia. A minimum, allowable pipe temperature slightly above the freezing point is taken for the cold-case design condition, $\hat{T}_2^* = 197.2$ K. Finally, it is assumed $(L_0, s) = (0, 0)$ in the absence of additional data. All of the data required to initiate design calculations are summarized in Table 3.

Note that the product bL_2 is in the range $12.01 < bL_2 < 13.16$. This observation allows the use of the approximation $\sinh bL_2 = \cosh bL_2 = 0.5\exp(bL_2)$, so that the four temperatures required to evaluate the several ψ parameters may be expressed in simplified form as Eqs. (30) shown in Table 4. Equations (26) and (27) may be adapted to the simplified form as shown in Eqs. (31), also listed in Table 4.

Using the hot case conditions and setting $\tilde{L}_1 = L_2$ (full condenser utilization), Eq. (30a) may be rearranged to find the maximum heat load, $\tilde{Q} = 22.14$ W. The mean temperatures follow from Eqs. (30b) and (30d) as $\bar{T}_1 = 313.19$ K and $\bar{T}_3 = 292.63$ K.

Equation (31b) may be solved for $\hat{L}_1$ using cold-case conditions to find $\hat{L}_1 = 0.7600$. This result, when used in Eq. (31a), leads to the heat load at incipient freezeout, $\hat{Q} = 16.61$ W. The mean temperatures as found from Eqs. (30b), (30c), and (30d) are $\bar{T}_1 = 300.84$ K, $\bar{T}_2 = 204.44$ K, and $\bar{T}_3 = 239.92$ K.

Using these values in Eq. (29), find $m_g R_g / V_c = 9692$ N/m^2 · K, $V_r/V_c = 2.563$, where $V_c = A_c l_3 = 26.25$ cm^3 and, for nitrogen, $R_g = 0.29696$ kJ/kg · K. The mass of N_2 and reservoir volume required for this VCHP application are $m_g = 0.8561$ g and $V_r = 67.28$ cm^3. Axial temperature profiles for the hot and cold cases are shown in Fig. 4; these profiles illustrate the sensitivity of VCHP freezeout to comparatively small changes in heat load when operating in a space-like environment.

Discussion

The two independent assumptions of specified heat flux and gas inventory based on zonal mean temperatures lead to analytical simplifications that retain accuracy for many engineering applications; however, the thermal analyst should be aware of the limits of the formulation. Specifically, the use of a specified flux $q(\zeta)$ in place of a specified internal film coefficient $h(\zeta;\text{internal})$ tends to mask the physics of heat pipe processes. To be sure, both $q(\zeta)$ and $h(\zeta;\text{internal})$ are artifices introduced for analytical convenience; however, $h(\zeta;\text{internal})$ retains the distinction between pipe wall (and/or wick) temperature and working fluid temperature. The model developed here introduces flux related parameters L_0, s, and n (the axial increase parameter) that must be estimated by empirical or intuitive means; n must be an integer to evaluate Eq. (12b) and is taken as $n=2$ for analytical convenience. The parameter s is bounded as $0 < s \le s(\max)$ where $s(\max)$ is the largest value that avoids a temperature maximum in the axial range $0 < z \le l_1$. It is reasonable to use $L_0 = 0$ for low-to-full heat loads (e.g., $Q > 0.1Q(\max)$) that require an active condenser length, $l_1 > 0$. It is not yet clear how L_0 behaves at very low heat loads or how it is related to heat load, radial heat loss through insulation, pipe axial thermal conductivity, and external heat loss coefficients h_a and h_i. The internal film coefficient will depend on wick configuration, wick material, vapor/gas cross-sectional area, working fluid, and noncondensable gas. At present, there are very few correlations available for $h(\zeta;\text{internal})$ and only a few equivocal guidelines[2,5] for general application. The use of this first-order model is justified on the basis of analytical convenience and numerical stability and on the scarcity of data for $h(\zeta;\text{internal})$.

The validation analysis based on data reported in Refs. 1 and 2 demonstrates the potential accuracy of the first-order formulation. However, it is not reasonable to expect such good conformance with test results or more exact diffuse front predictions under all conditions. In a sense, the VCHP of Refs. 1 and 2 provides a severe test of the present formulation because there was no temperature controlled gas reservoir (i.e., $V_r = 0$). On the other hand, the environment was benign and axial conduction was low, so that the active and inactive condenser sections were isothermal at their respective temperature levels over comparatively long distances. The bimodal isothermal regions are well represented by their respective mean temperatures; only run 1 (full heat load) had a nonisothermal inactive condenser. In run 1, approximately 29% (by mass) of the gas was in the active condenser and 71% in the inactive section. In the other runs, approximately 10% or less was in the active condenser. In the numerical example previously described, the gas mass distribution was as shown in Table 5. The hot case distribution of gas seems reasonable in consideration of the monotonic temperature profile; however, the cold-case distribution shows a relatively large mass in the strongly nonisothermal inactive sections. Clearly, engineering judgment is required in dealing with similar nonmonotonic, nonisothermal heat pipes.

The validation analysis showed that $s = 0$ for the stainless steel/water/air VCHP when operating at low-to-full heat loads. This value implies $q(\zeta) = h(\zeta;\text{internal})[T(\zeta)_{\text{vapor}} - T(\zeta)_{\text{wall}}] = q_0$, a constant in the active condenser section. Presumably, anything that has an influence on $h(\zeta;\text{internal})$, $T(\zeta)_{\text{vapor}}$, or $T(\zeta)_{\text{wall}}$ will also have an influence on s. The discussion above identified several conditions that may influence $h(\zeta;\text{internal})$. Additional conditions that may influence vapor and wall temperatures include pipe diameter, pipe wall thickness, pipe and wick material, and external fins. Large-diameter pipes may be more sensitive to two-dimensional heat and mass transfer effects, while wall thickness, material, and external fins will influence the magnitude of axial conduction.

Table 5 Gas mass distributions

Location	Hot case %	Cold case %
Reservoir	94.9	79.4
Active condenser	0.8	6.9
Inactive condenser	—	4.9
Second adiabatic section	4.3	8.8

The results of Refs. 1 and 2 indicate that the use of a single mean heat loss coefficient, $h_a = h_i = h$ was adequate for the operating conditions. The present numerical example used a uniform loss coefficient for illustrative purposes only. The assumption of uniform loss coefficient would not be appropriate for a true spacecraft design application. For example, linear radiation leads to the relationship

$$h = h(T, T_\infty) = \sigma\mathcal{F}\left(T^2 + T_\infty^2\right)\left(T + T_\infty\right)$$

In the numerical example for the cold case, $h_a = h(\bar{T}_1, \hat{T}_\infty)$ and $h_i = h(\bar{T}_2, \hat{T})$ and it can be found that $h_a/h_i = 2.39$. This sizable difference in heat-transfer coefficients suggests the use of the complete solution for A_1, A_2, B_2, and A_3 implicit in Eqs. (12) and (13); the assumption of uniform film coefficients should be used only for approximate solutions.

Conclusions and Recommendations

The first-order model provides succinct, explicit expressions that relate evaporator temperature, heat load, reservoir temperature, heat pipe geometry, and environmental conditions. The formulation presented here may be adapted for designing variable-conductance heat pipes (VCHPs) and predicting their performance for many terrestrial and spacecraft applications.

The analytical model postulates the use of two parameters that can be determined empirically. The location at which condensation starts, $z = -l_0$, in the adiabatic section and the heat flux distribution parameter s may be evaluated from test data. It is believed that $l_0 = 0$ is suitable for most applications for a VCHP operating at low-to-full heat loads. The value $s = 0$ appears to represent a lower bound; an upper bound may be found by seeking $s = s(\max)$ such that $s > s(\max)$ predicts a temperature maximum in the active condenser for $z > 0$. Additional test data are required to develop quantitative relationships among l_0, s, heat load, wall thermal conductivity, and environmental conditions. In the absence of more information, it is recommended that the first-order formulation be limited to heat loads $Q > 0.1Q(\max)$ with $l_0 = 0$ and the value of s should be selected in the range of $0 < s < s(\max)$.

It is recommended that additional tests be performed to obtain reliable data on VCHP operation at very low heat loads ($L_1 < 0$) and at excessive heat loads. The problem of the overloaded VCHP, with the possibility of condensation in the secondary adiabatic section and in the reservoir, deserves both analytical and experimental attention.

References

[1]Edwards, D.K. and Marcus, B.D., "Heat and Mass Transfer in the Vicinity of the Vapor-Gas Front in a Gas Loaded Heat Pipe," *Journal of Heat Transfer*, Vol. 94C, No. 2, May 1972, pp. 155-162.

[2]Marcus, B.D., "Theory and Design of Variable Conductance Heat Pipes," NASA CR-2018, April 1972.

[3]Shimoji, S., Kimura, H., and Matsushita, T., "Prediction of Evaporator Temperature of a Gas Loaded Heat Pipe by the Diffuse Front Model," AIAA Paper 78-410, May 1978.

[4]Edwards, D.K., Fleischman, G.L., and Marcus, B.D., "Users Manual for TRW GASPIPE 2 Program: A Vapor-Gas Front Analysis Program for Heat Pipes Containing Noncondensable Gas," NASA CR-114672, Oct. 1973.

[5]Brennan, P.J. and Kroliczek, E.J., "Heat Pipe Design Handbook," prepared for NASA Goddard Space Flight Center, under Contract NAS5-23406, June 1979.

[6]Sun, K.H. and Tien, C.L., "Simple Conduction Model for Theoretical Steady-State Heat Pipe Performance," *AIAA Journal*, Vol. 10, Aug. 1972, pp. 1051-1057.

[7]Bobco, R.P. "Variable Conductance Heat Pipes: A First Order Model," AIAA Paper 85-0935, June 1985.